Chapter 3

Oxygen reduction reaction on nitrogen-doped graphene activated by co-doped oxygen functional groups

Nitrogen-doped carbon materials have gained considerable attention as non-platinum-group catalysts for oxygen reduction reaction (ORR). However, there has been much controversy about the active sites, not only concerning the different nitrogen doping configurations but also the correlation of activity with nitrogen dopants. Here, nitrogen dopants are systematically introduced into a monolayer graphene – a model carbon-based catalyst – to reveal the potential active sites for oxygen reduction catalysis. Upon nitrogenation treatment, pure graphene with minimal surface oxidation shows decreased ORR activity, while a graphene surface containing air-induced oxidation sites enhances the activity. Regardless of the nitrogen dopants, graphene exhibits improved catalytic activity upon oxygen doping. Further correlation of the chemical compositions with the catalytic activity of nitrogenated and oxygenated graphene reveals for the first time that oxygen containing groups, instead of N-doping sites, are at the origin of the enhanced activity of nitrogenated graphene for ORR electrocatalysis.

This chapter is prepared as an article: Lin Jiang, Bas van Dijk, Longfei Wu, Jan P. Hofmann, Viorica Tudor, Marc T. M. Koper, Dennis G. H. Hetterscheid, Grégory F. Schneider, submitted.

3.1 Introduction

Nitrogen-doped (N-doped) carbon-based metal-free materials like graphene and carbon nanotubes have been reported as effective and promising alternatives to platinum catalysts for the oxygen reduction reaction (ORR), a critical reaction for renewable energy technologies including fuel cells.[1] Both experimental and theoretical efforts have been devoted to determine the active sites of N-doped carbon materials for the ORR.[2] Particularly, positively charged carbon atoms next to pyridinic nitrogen atoms have been suggested to preferentially adsorb O_2 molecules and thus favor fast ORR kinetics.[3] However, such a mechanism does not explain the catalytic effect in boron and/or sulphur doped carbon materials.[4] Moreover, it has been reported that in some cases graphene containing N dopants, such as chemical vapor deposited (CVD) graphene with dominantly pyridinic N dopants, are not active for the ORR.[2b, 5] In fact, graphene with vacancy defects is in some cases more active than N-doped graphene towards the ORR.[5b, 6] The controversy about the ORR activity of N-doped graphene can be ascribed to the significant structure and morphology variations in the studied materials, which are mostly based on graphene nanoflakes dispersions.[7] Typically overlooked issues for these materials are the inhomogeneous and undervalued active sites for ORR catalysis, caused by flake aggregation, irreversible pyrolysis or vigorous chemical treatments. For example, oxygen groups are abundant in graphene nanoflakes due to their high oxygen affinity. In fact, oxygen-containing functionalities in carbon nanotubes and reduced graphene oxide have been reported to directly correlated to the active ORR performance.[8] In addition, a recent computational paper describing proton-coupled electron transfer on graphene surfaces showed that carbene type active sites are stabilized by a combination of pyridinic nitrogen and quinone type oxygen functionalities.[9] However, little experimental attention has been given to the role of oxygen functionalities within N-doped graphene in the ORR mechanism.

Therefore, a detailed study disclosing the relationships between ORR activity and the surface chemistry of N-doped carbon materials is desired. For that purpose, a reliable and well-defined system is required. Consequently, monolayer graphene film grown via the chemical vapor deposition (CVD) method were used in this study.[10] Homogeneous graphitization level and sensitive surface chemistry make the monolayer CVD graphene an ideal model for carbon-based metal-free catalysts.[11] Specifically, ORR performance of a monolayer graphene upon N- and O-doping was systematically studied. Indeed, this N-doped graphene has a high level of graphitization and conductivity as characterized by Raman spectroscopy and electrical transport measurements. To study the electrochemical performance for ORR catalysis, both an epoxy resin and a rotating glassy carbon disk electrode were

used as the support of the graphene. According to the XPS characterization, it is found that oxygen functional groups (C-O), instead of nitrogen dopants, are the most active sites for oxygen reduction on nitrogenated graphene.

3.2 Results and Discussion

3.2.1 Raman characterization of N-doped graphene

Raman spectroscopy (Figure 3.1a) was conducted to evaluate the N-doping process on chemical vapor deposition (CVD) graphene supported by a SiO_2/Si substrate. For pristine graphene, two main characteristic peaks for monolayer graphene can be found. The G peak (~1580 cm^{-1}) arises from the C-C stretching within all sp^2 carbon systems. The sharp 2D peak (~2670 cm^{-1}) corresponds to the overtone of breathing modes of six-atom rings and is sensitive to the number of graphene layers and doping effect.[12] After more than 2 s of nitrogenation, a D peak appears at ~1340 cm^{-1} that corresponds to single phonon intervalley scattering events and is associated with the incorporation of nitrogen atoms into the lattice of graphene as defect sites.[13] Upon longer nitrogenation times (> 6 s), a D' peak at 1620 cm^{-1} emerges as a shoulder of the G peak due to the intervalley scattering induced by nitrogen defects.[14] When the nitrogenation time increases from 0 to 60 s, the intensity ratio $I(2D)/I(G)$ decreases from 2.0 to 0.7 (Figure 3.1b) and the 2D peak shifts from 2674 to 2665 cm^{-1} (Figure 3.1c), both suggesting an electron (n-) doping effect in nitrogenated graphene.[15] The full width at half maxima (FWHMs) for the D, G and 2D peaks (Figure 3.1d) slightly increase upon increasing the nitrogenation time from 0 to 30 s and saturate at 60 s. The increase of the FWHMs indicates a growth of defect density. As a quantitative reflection of the defect density (n_D) and interdefect distance (L_D),[16] the ratio of $I(D)/I(G)$ in Figure 3.1d (black line) exhibits a similar growth trend with the peak widths (see n_D and L_D in Table AII. 1). Such consistent saturation trends may correspond to the clustering of nitrogen defects at high doping level.[5a, 17] This is reflected by a domain-like defect distribution in graphene after 30 s of nitrogenation (Figure AII. 1). Specifically, the increasing trends for both the $I(D)/I(G)$ ratio and the FWHM of the G peak confirm the dominance of sp^2-hybridized carbon network over the introduced defects, thus it is concluded that the N-doped graphene still has a high lattice integrity. It is reported that a ratio of circa 3 for $I(D)/I(D')$ represents boundary defects while a ratio of circa 7 indicates vacancy defects as based on a model of uniform defect distribution without clustering.[18] In our case, the $I(D)/I(D')$ ratios vary from 6.5 (10-20 s of nitrogenation) to 5 (more than 30 s of nitrogenation) (Figure 3.1d, blue dots) indicating that nitrogen dopants behave more like vacancy defects. To conclude, Raman spectroscopy shows that N-doped graphene has a high, uniform graphitization level and vacancy-like defects.

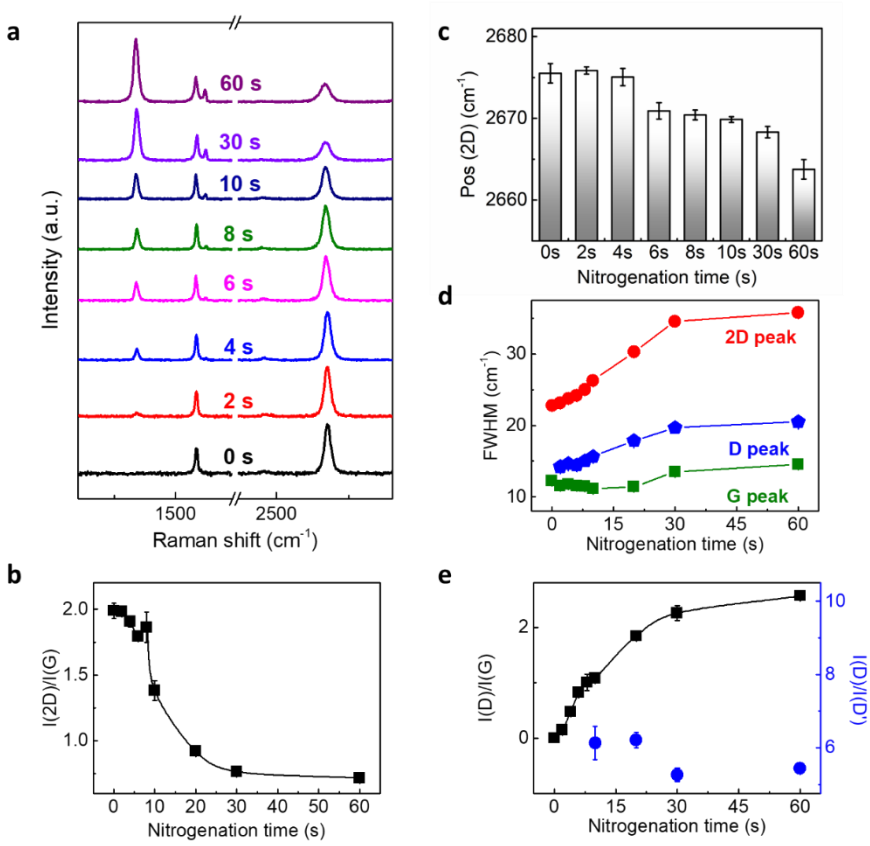

Figure 3.1 Raman spectroscopy of N-doped graphene. a) Raman spectra of exfoliated graphene after 0-60 s of nitrogenation. The spectra are recorded using 2.33 eV (532 nm) laser excitation. b) Intensity ratio $I(2D)/I(G)$ as a function of nitrogenation times. c) Red-shift of 2D peak position vs nitrogenation times. d) Variations of full width at half maxima (FWHMs) for D, G and 2D peaks upon 0 to 60 s nitrogenation. e) Evolution of intensity ratio $I(D)/I(G)$ (black) and $I(D)/I(D')$ (blue) with respect to the nitrogenation time.

3.2.2 Structure characterization of N-doped graphene

X-ray photoelectron spectroscopy (XPS) characterization was further performed to analyze the chemical structure of nitrogenated graphene. XPS survey spectra for pristine and 60 s N-doped graphene are displayed in Figure AII. 2a-b, with O1*s* peaks mainly originating from the underlying copper substrate. Figure 3.2 shows the high resolution XPS C1*s* (a) and N1*s* (b) spectra for pristine, 30 s and 60 s of N-doped graphene. The C1*s* spectra can be deconvoluted into five peaks: sp^2 C-C (284.4 eV), sp^3 C-C (285.0 eV), C-O/C=N (286.4 eV), C=O/C-N (288.0 eV), and O-C=O (289.0 eV), respectively.[19] The oxygen-containing groups in C1*s* indicate oxidation in pristine graphene induced by air exposure (even for a short period). A higher content of

oxygen in aged graphene samples (Figure AII. 2c) confirms the unavoidable oxidation during handling. As a result, to obtain reliable comparisons of the chemical structure, fresh graphene samples with similar aging degrees (i.e. within one week after the CVD growth) were used for different doping treatments. Upon nitrogenation, the O:C ratio evolves from 2.3% for pristine, to 4.2% and 10.2% for 30 s and 60 s N-doped graphene, respectively. Nitrogenation treatments create high reactive sites for oxygen uptake, which explains the increased oxidation degree of N-doped graphene.[20] Specifically, vacancy defects that are created during the more clustered N-doping process (30 to 60 s nitrogenation times) are mainly responsible for the increased oxidation. The N 1*s* spectra for 30 s N-doped samples consist of two main peaks centered at 398.9 eV and 399.9 eV, corresponding to pyridinic (pyrid-) and pyrrolic (pyrro-) N.[5b, 19a] For 60 s N-doped graphene, in addition to the pyrid- and pyrro-N peaks, another peak at 401.1 eV is observed and assigned to quaternary (quat-) N. Moreover, the dominant forms of pyrid- and pyrro-N agree well with the observed n-type doping effect in Figure 3.1 (see Figure AII. 1).

3.2.3 Electrical transport characteristics of N-doped graphene

Next, the electron transport characteristics of graphene was studied in the configuration of an electrochemically-gated graphene field effect transistor (GFET) that was fabricated following a previously reported facile strategy (see Methods).[21] An epoxy substrate was used to support a clean, pristine graphene surface that was protected by a clean and annealed copper substrate. Moreover, this graphene surface was never in contact with and thus contaminated by any polymer that is generally used for graphene transfer,[22] and was only exposed to the ambient oxygen in a short period before measurements. The surface purity is better than that of graphene transferred by the polymer assisted method as the graphene contains a lower density of charged impurities (i.e. originating from ambient oxidation or trapped impurities).[21] The conductance (G) of this clean graphene demonstrates an ambipolar behavior with respect to the gate voltage (V_g) as shown in Figure 3.2c (black line) (see discussion in Appendix II. 3). The G (V_g) curves start to shift negatively after 10 s of nitrogenation and the charge neutrality point (CNP) shifts by -30 to -60 mV between 20 to 60 s of nitrogenation. This shift suggests an n-doping effect in graphene (Figure 3.2d). Using the capacitor model in the electrochemical-gating configuration[23], it is found that the carrier mobility (μ) of pristine graphene decreases from ~3800 $cm^2 V^{-1} s^{-1}$ to ~550 $cm^2 V^{-1} s^{-1}$ after 30 s of nitrogenation and subsequently levels off at 60 s of nitrogenation (Figure 3.2d, black). Notably, the high carrier mobility value for pristine graphene confirms its intrinsic high-quality and surface purity. Corresponding to the similar saturation trend of $I(D)/I(G)$ ratios in Figure 3.1d, graphene carrier mobility is predicted to be closely related to the

distribution of nitrogen dopants. At low doping levels (< 30 s nitrogenation), nitrogen atoms independently implant into the carbon lattice, resulting in a rapid conductivity degradation of graphene. In contrast, at high doping levels (between 30 and 60 s nitrogenation), clustering at the pre-existing nitrogen doping sites occurs and results in no further degradation of the conductivity of graphene. Moreover, the large decrease of the minimum conductivity $G_{\min}$ from 0 to 30 s nitrogenation and stable value of $G_{\min}$ between 30 to 60 s of nitrogenation (Figure 3.2e) further confirm that nitrogenated defects are the dominating scatterers for the charge carriers in graphene.[24] These observations reveal that nitrogen dopants in the monolayer graphene lattice cause significant intervalley scattering, reduce the carrier mobility and (minimum) conductivity, and negatively shift the CNP by inducing an n-doping effect.

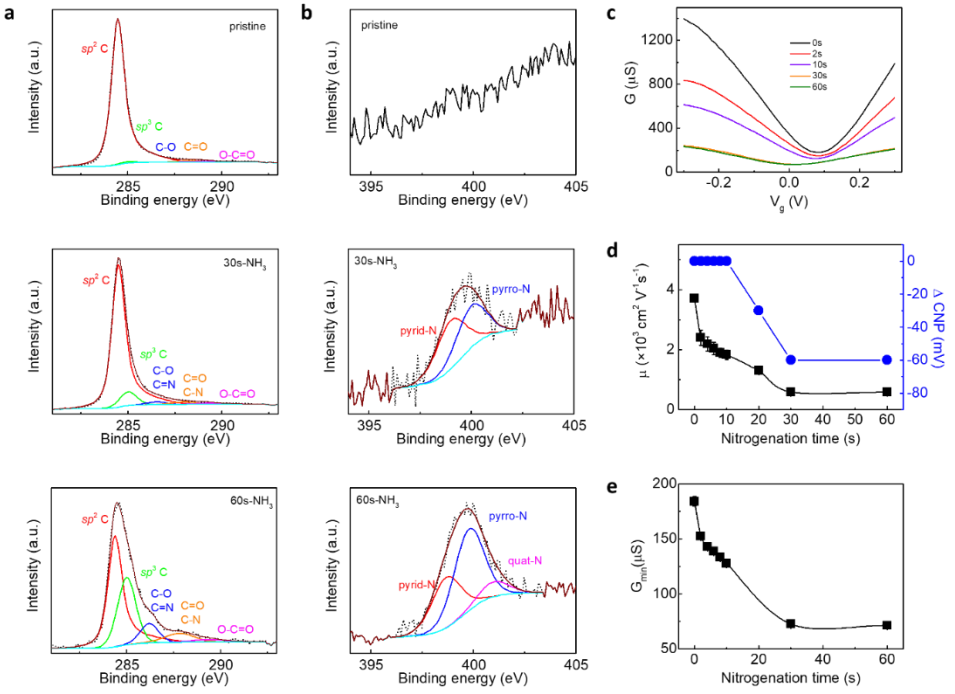

Figure 3.2 Electronic/structural characterization of N-doped graphene. a) C1*s* core level high-resolution XPS spectra of pristine, 30 s and 60 s N-doped graphene. b) N1*s* core level spectra of pristine, 30 s and 60 s N-doped graphene. All the spectra were collected from the CVD graphene as grown on copper foil in a fresh status (i.e. within one week after the CVD growth). c) Conductance (G) vs the gate voltage (V_g) curves of graphene upon nitrogenation time from 0 to 60 s. The electrolyte solution is 0.1 M KCl with 10 mM Tris (pH 8). d) The carrier mobility of graphene (μ, black square) and charge neutrality point (CNP, blue dot) evolve with the nitrogenated times. e) The minimum conductance ($G_{\min}$) as a function of the nitrogenation time.

3.2.4 ORR activity of N-doped and O-doped graphene

The ORR activity was first studied with the clean graphene surface on the epoxy substrate (illustrated in Figure AII. 3a), which was also used for the transport measurements described in the previous section.[21] In this setup, the well-defined monolayer graphene is the only catalytic surface available to perform the ORR, and is referred to as pure graphene. More importantly, the obtained pure graphene samples were tested as fresh as possible, to minimize air contaminations (i.e. oxidation or hydrocarbon adsorption).[21, 25] As will be shown later, the ORR polarization curves can also reflect sample freshness and reliability. Figure 3.3 shows the cyclic voltammograms (CVs) and the linear sweep voltammograms (LSVs) of the pure graphene in 0.1 M H_2SO_4 and 0.1 M NaOH solution saturated with O_2 in a stationary configuration. A more positive onset potential in alkaline medium (~0.68V) than in acidic medium (~0 V), and a higher current density (~4-fold at –0.2 V) in 0.1 M NaOH shows the higher ORR activity in alkaline medium (Figure 3.3a). It is well known that carbon-based catalyst are more active for the ORR in alkaline media. This is most likely due to $O_2^{-\cdot}$ being the first intermediate in the mechanism of ORR, which is formed by an electron transfer reaction that is not coupled to proton transfer and therefore does not scale linearly with the RHE reference scale.[26] The LSV curves in alkaline medium have an extra reduction peak at ca. 0.45V. This peak is ascribed to oxygen reduction catalyzed by the oxygen-containing groups present on the surface of graphene and other carbon electrodes including glassy carbon.[27] In addition, more aged pristine graphene showed increased current in this region (Figure AII. 4a). Therefore, only pristine graphene samples producing similar or lower peak currents at 0.45 V compared to the LSV in Figure 3.3a are used for doping treatment studies. Upon nitrogen doping from 0 to 60 s, the catalytic current densities are observed to decrease monotonically both in acidic (Figure 3.3b) and in alkaline medium (Figure 3.3c). This is in contrast with the earlier reports that claim that n-doping of nitrogenated graphene improves ORR activity by creating Lewis basic sites which enhance initial O_2 adsorption.[2a, 3] In our case, the observed decrease in ORR activity of graphene after nitrogenation suggests that the N-doping sites within the graphene surface do not contribute to the generation of active catalytic sites. In fact, recent reports support the observation that the catalytic activity of graphene decreases upon nitrogenation.[5] For example, N-doped graphene was reported to show similar ORR activity with pristine graphene.[5b] A theoretical study proposes that the nitrogen atoms in N-doped graphene could actually hinder the adsorption of oxygen molecules onto the graphene surface due to their higher electron density.[28]

Inspired by the recent work that oxygen-containing groups in carbon-based materials are closely related to the active ORR performance,[2a, 3] oxygen groups via oxygen

plasma treatment was further co-doped into the nitrogenated graphene. As illustrated in Figure 3.3d, the ORR activity for 60 s nitrogenated graphene is decreased as compared to pristine graphene. In contrast, co-doped graphene that is treated by both 60 s nitrogenation and 10 s of oxygenation enhances the ORR activity. However, more oxygen doping in the co-doped graphene (60 s nitrogenation and 30 s oxygenation) impairs the positive effect of oxygen doping on the ORR activity. Apparently, nitrogenated graphene is only active for ORR catalysis in the presence of a certain amount of co-doped oxygen groups.

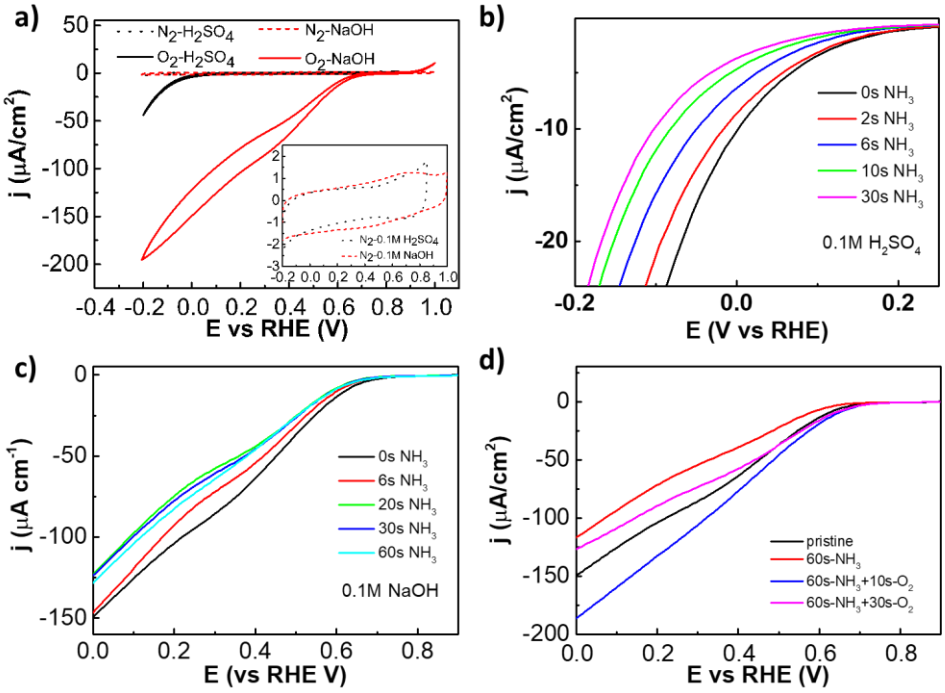

Figure 3.3 ORR activity on the pure graphene upon nitrogenation and oxygenation treatments. a) Cyclic voltammetry (CV) curves of monolayer graphene in 0.1 M H_2SO_4 and 0.1 M NaOH solutions saturated with N_2 and O_2, respectively. b) Linear sweep voltammetry (LSV) polarization curves of graphene upon 0 to 30 s of nitrogenation in O_2-saturated 0.1 M H_2SO_4. c) LSV curves of graphene upon 0 to 60 s of nitrogenation in O_2-saturated 0.1 M NaOH. d) Comparison of LSV curves in O_2-saturated 0.1 M NaOH for pristine graphene, nitrogenated graphene (60s-NH_3), and graphene co-doped with nitrogen and oxygen (60s-NH_3+10s-O_2) and 30 s (60s-NH_3+30s-O_2).

3.2.5 ORR kinetics and selectivity of N-doped and O-doped graphene

A rotating ring-disk electrode (RRDE) method was further employed to gain insights into the product selectivity and the ORR kinetics of nitrogenated graphene. The current was measured at both the glassy carbon (GC) disk and the platinum ring. The

Pt ring was held at a potential of 1.2 V, to oxidize ORR products such as hydrogen peroxide HO_2^- (the form of H_2O_2 in alkaline medium) and/or superoxide $O_2^{-\cdot}$. Graphene was transferred onto the GC disk via the traditional polymer assistant method (see Figure AII. 3b and Methods).[22] Importantly, the opposite face of graphene is exposed as compared to the previously described graphene on epoxy substrate (pure graphene). XPS analysis reveals that this graphene surface contains oxygen functionalities, which is probably due to air-induced contaminations and oxidation (Figure 3.2). As shown in Figure 3.4a, a monolayer graphene on the GC disk decreases the ORR current compared to that of bare GC, indicating that fewer active sites are available on the graphene surface. Furthermore, bilayer graphene on GC has an even more reduced ORR current compared to the monolayer graphene. This implies that the GC as the underlying substrate has a certain influence on the catalysis of the graphene overlayer, for instance through cracks in this monolayer graphene film. In contrast, the bilayer graphene displays better reproducibility and reliability (see Figure AII. 4 and Appendix II. 4). Therefore, the bilayer graphene was used for the RRDE measurements and referred to as RRDE graphene. Compared to the LSV of pure graphene, RRDE graphene (at 0 rpm) has a more pronounced peak at 0.45 V (Figure 3.4b). As previously described, this feature relates to a higher surface oxidation of RRDE graphene as compared to pure graphene.

Under rotating conditions from 400 to 1000 rpm, the LSV of bare GC in O_2 saturated 0.1 M NaOH shows increasing disk and ring currents (Figure 3.4c). Fully diffusion-limited currents were never reached at the GC disk nor for RRDE graphene (*vide infra*), neither for HOPG as was reported previously.[3] Figure 3.4d shows the LSV curves of RRDE graphene before (as the pristine sample) and after nitrogenation and oxygenation treatments. The ORR activity of 30 s nitrogenated RRDE graphene (N30) is slightly decreased as compared to pristine graphene. In contrast, 60 s nitrogenated graphene (N60) shows significantly increased ORR activity. Likewise, 10 s oxygenated graphene (O10) also displays an improved current, indicating that nitrogen atoms in graphene are not necessary for enhanced ORR activity. The co-doped graphene with 30 s of nitrogenation and 10 s of oxygenation (N30-O10) demonstrates the highest current among all the doped samples. Of note, the increased ORR current for N60 RRDE graphene conflicts with the decreased activity found for the corresponding pure graphene (see Figure 3.3c). As stated before, RRDE graphene has more oxygen containing groups than pure graphene due to the differently exposed faces of graphene. A different explanation is that vacancy defects, that are generally generated together with N dopants, might expose the underlying GC disk and thus GC could contribute to the ORR activity for the RRDE graphene. To test this possibility, the ORR currents of N60 graphene (on RRDE), a bare GC disk and partially

exposed GC (from 10% to 50% in terms of area) were compared (Figure AII. 5). Due to the large amounts of defects and oxygen functionalities, bare GC exhibits a distinct polarization curve with a prominent extra peak at ca. 0.45 V. In contrast, N60 graphene exhibits a much larger ORR current at high overpotential (near 0 V vs RHE) and a relatively lower current at 0.45 V compared to all partially exposed GC electrodes. It can therefore be concluded that the underlying GC substrate plays a negligible role in the ORR activity of N60 RRDE graphene.

The RRDE method allows for product selectivity studies by using both the Koutecky-Levich method and by comparing currents obtained on the ring and on the disk ($I_{\mathrm{ring}}/I_{\mathrm{disk}}$, see Appendix II. 5). At the ring, both superoxide $O_2^{-\cdot}$ and hydrogen peroxide H_2O_2 can be oxidized. Higher ratios of $I_{\mathrm{ring}}/I_{\mathrm{disk}}$ reflect higher selectivity towards $O_2^{-\cdot}$ and H_2O_2, while in return lower ratios indicate that more H_2O may be produced. In Figure AII. 8b, the selectivity is calculated based on the current values in the potential range of 0~0.1 V with a collection efficiency of 22.5% at the ring (see Figure AII. 6 and Appendix II. 5). The $I_{\mathrm{ring}}/I_{\mathrm{disk}}$ ratio is as low as 36% for bare GC, which is traditionally known to reduce O_2 to HO_2^- with 100% through a $2e^-$ pathway.[29] The observed lower ratio suggest that the collection efficiency of HO_2^- is underestimated by the RRDE technique, as the oxidation of HO_2^- at the platinum ring is surface dependent and therefore not fully mass transport limited. Therefore, the collection efficiency can be lower than that for the ferricyanide.[30] In comparison to GC, pristine graphene exhibits a higher selectivity ratio of 47%. Similar ratios are found for N30 (~48%) and N60 (~47%), while slightly decreased ratios for O10 (~45%) and N30-O10 (~42%) are found. The higher selectivity ratios on pristine and doped graphene samples suggest that more superoxide might be produced (it is anticipated that superoxide, in contrast to peroxide, is oxidized via an outer-sphere reaction), which agrees well with the lower *n* values (~1.6 – 1.8). Most likely, most active sites produce HO_2^- and/or $O_2^{-\cdot}$ but no clear correlation was found with the presence of certain nitrogen and/or oxygen functionalities.

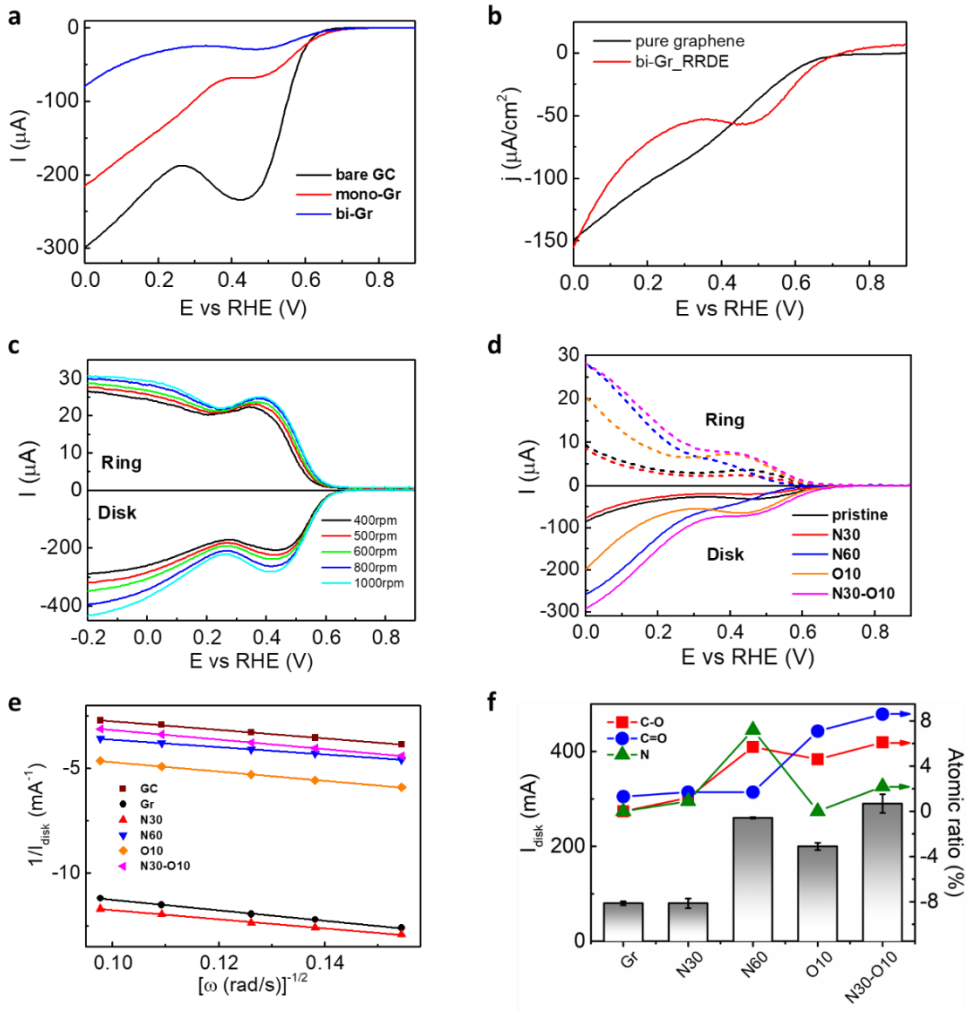

Figure 3.4 ORR activity and selectivity of N-doped graphene. a) LSV curves of bare GC, monolayer (mono-Gr) and bilayer (bi-Gr) graphene on the GC disk at 600 rpm. b) Polarization curves of a pure graphene supported by epoxy substrate and a (bilayer) RREDE graphene on the GC without rotation. c) Polarization curves of bare GC and ring electrode at rotation speed varying from 400 to 1000 rpm. d) Polarization curves of graphene after nitrogenation and/or oxygenation and simultaneous H_2O_2 detection currents at the ring electrode (at 800 rpm). "Pristine" denotes the pristine RRDE graphene. "N30" and "N60" represent 30 s and 60 s of nitrogenated graphene, respectively, while "O10" for 10 s of oxygenated graphene. e) Koutecky-Levich plots of different doped graphene samples at 0 V. f) Correlation of cathodic currents at 0 V with atomic ratios (%) of C-O, C=O and N dopants for the different doped graphene samples. All the ORR experiments were performed in 0.1 M NaOH solutions saturated with O_2.

The Koutecky-Levich method (Figure 3.4e) confirms the best ORR activity on the co-doped sample (N30-O10) while the lowest activity on the pristine and N30 graphene. The origins of the Koutecky-Levich plots are summarized in Figure AII. 7. Based on the Koutecky-Levich curves, we calculate the electron transfer number (*n*) per O_2 molecule in the potential window of 0 to 0.2 V for the GC and different graphene surfaces. In contrast to bare GC which has an *n* value of 2 (Figure AII. 8a), pristine graphene has a lower value of 1.6, indicating the formation of less reduced products, i.e. $O_2^{-\cdot}$ ($1e^-$). After doping treatments, the *n* value rises to 1.8 for most of the N- or O-doped samples suggesting that the heteroatoms doping may improve the selectivity of $2e^-$ or even $4e^-$ processes and thus produce more H_2O_2 and/or H_2O. Particularly, the largest *n* value of 2.3 for N60 suggests a higher selectivity for H_2O ($4e^-$) as product. The presence of quat-N only in 60 s N-doped graphene is the origin of this selectivity and agrees well with reports stating that quaternary nitrogen at the edge sites is positively related to this 4e pathway.[2a]

Table 3.1 XPS analysis results for different doped graphene samples

samples	N/C (%)	Concentrations of species (%)									
		*sp*² C 284.4eV	*sp*³ C 285.0eV	C–O/C=N 286.4eV		C=O/C–N 288eV		O-C=O 289.5eV	Pyrid-N 398.9eV	Pyrro-N 399.9eV	Quat-N 401.1eV
Pristine	0	96.6	1.1	0	0	1.3	0	1.0	–	–	–
N30	1.0	86.8	7.2	1.2	0.5	1.7	0.4	1.3	0.5	0.4	–
N60	7.7	47.3	29.0	5.7	2.7	1.7	4.5	2.1	2.4	4.5	0.3
O10	0	76.2	7.4	4.6	0	7.1	0	4.7	–	–	–
N30-O10	2.3	68.4	8.4	6.1	0.6	8.6	1.6	4.0	0.6	1.6	–

3.2.6 Identification of ORR catalytic sites in N-doped and O-doped graphene

The same graphene surfaces used for RRDE experiments were analyzed by XPS as well. This way, the ORR activity can be correlated with the chemical structures of different doped graphene samples. Table 3.1 summarizes the concentrations of different C and N species and their relative ratios (the C1*s* spectra of O10 and N30-O10 graphene are displayed in Figure AII. 2d-e). As shown in the C1*s* deconvolution, the binding energies of C-O and C=O overlap with that of C=N (pyrid- and quat-N) and C-N (pyrro-N), respectively. By calibrating the atomic ratios according to the peak areas and relative sensitivity factor (RSF), the respective atomic ratios (abbreviated: at.%) for C-O and C=O groups are obtained. Figure 3.4f shows the correlations of the ORR activities of different doped graphene samples with their corresponding atomic ratios of C-O, C=O and N atoms. The disk currents at 0 V vs RHE increase with the

percentage of C-O whereas no apparent correlation with the content of C=O or N dopants is found. The high atomic ratios of C-O in N60 graphene as well as the improved activity in O10 samples both suggest that nitrogen functionalities are of less relevance for the ORR activity as compared to C-O groups. In other words, C-O functionalities in nitrogenated graphene are responsible for enhanced ORR activity. To the best of our knowledge, this is the first experimental evidence revealing that oxygen containing groups, instead of nitrogen atoms, are the origin for improved ORR electrocatalysis in nitrogenated graphene.

3.3 Conclusions

In summary, nitrogenation and oxygenation of graphene have been systematically controlled for the investigation of the corresponding impacts on its electrical properties and ORR performance. Characterized by Raman spectroscopy and transport measurements, after nitrogenation treatments graphene preserves a high graphitization level and lattice integrity with an n-doping effect. Graphene supported by epoxy substrate is found to be inactive for ORR upon nitrogen doping unless oxygen groups are introduced as co-doping contents. In contrast, RRDE graphene exhibits enhanced ORR activity after the same nitrogenation treatments due to the higher amount of surface oxidation. Further structure-activity correlations obtained from the RRDE system reveal that singly bonded carbon-oxygen groups rather than the N-doping sites in nitrogenated graphene are positively correlated to the enhanced ORR activity. In this study, C-O groups in the basal plane of nitrogenated graphene are pinpointed as the active sites for the ORR. Furthermore our work shows that research into nitrogen-doped graphene for enhanced ORR catalysis should critically evaluate the role of oxygen impurities.

3.4 References

[1] a) K. Gong, F. Du, Z. Xia, M. Durstock, L. Dai, *Science* **2009**, 323, 760; b) J. Shui, M. Wang, F. Du, L. Dai, *Sci. Adv.* **2015**, 1, e1400129; c) Y. Ito, H. J. Qiu, T. Fujita, Y. Tanabe, K. Tanigaki, M. Chen, *Adv. Mater.* **2014**, 26, 4145; d) L. Qu, Y. Liu, J.-B. Baek, L. Dai, *ACS Nano* **2010**, 4, 1321.

[2] a) H. B. Yang, J. Miao, S.-F. Hung, J. Chen, H. B. Tao, X. Wang, L. Zhang, R. Chen, J. Gao, H. M. Chen, *Sci. Adv.* **2016**, 2, e1501122; b) L. Lai, J. R. Potts, D. Zhan, L. Wang, C. K. Poh, C. Tang, H. Gong, Z. Shen, J. Lin, R. S. Ruoff, *Energy Environ. Sci.* **2012**, 5, 7936; c) T. Wang, Z.-X. Chen, Y.-G. Chen, L.-J. Yang, X.-D. Yang, J.-Y. Ye, H.-P. Xia, Z.-Y. Zhou, S.-G. Sun, *ACS Energy Lett.* **2018**, 3, 986.

[3] D. Guo, R. Shibuya, C. Akiba, S. Saji, T. Kondo, J. Nakamura, *Science* **2016**, 351, 361.

[4] Y. Zheng, Y. Jiao, L. H. Li, T. Xing, Y. Chen, M. Jaroniec, S. Z. Qiao, *ACS Nano* **2014**, 8, 5290.

[5] a) Z. Luo, S. Lim, Z. Tian, J. Shang, L. Lai, B. MacDonald, C. Fu, Z. Shen, T. Yu, J. Lin, *J. Mater. Chem.* **2011**, 21, 8038; b) Y. Jia, L. Zhang, A. Du, G. Gao, J. Chen, X. Yan, C. L. Brown, X. Yao, *Adv. Mater.* **2016**, 28, 9532.

[6] Y. Jia, L. Zhang, L. Zhuang, H. Liu, X. Yan, X. Wang, J. Liu, J. Wang, Y. Zheng, Z. Xiao, *Nat. Catal.* **2019**, 2, 688.

[7] a) Q. Li, S. Zhang, L. Dai, L.-s. Li, *J. Am. Chem. Soc.* **2012**, 134, 18932; b) L. J. Cote, F. Kim, J. Huang, *J. Am. Chem. Soc.* **2008**, 131, 1043.

[8] a) Z. Lu, G. Chen, S. Siahrostami, Z. Chen, K. Liu, J. Xie, L. Liao, T. Wu, D. Lin, Y. Liu, *Nat. Catal.* **2018**, 1, 156; b) H. W. Kim, M. B. Ross, N. Kornienko, L. Zhang, J. Guo, P. Yang, B. D. McCloskey, *Nat. Catal.* **2018**, 1, 282.

[9] L. R. Radovic, A. J. Salgado-Casanova, *Carbon* **2018**, 126, 443.

[10] L. A. Belyaeva, W. Fu, H. Arjmandi-Tash, G. g. F. Schneider, *ACS Cent. Sci.* **2016**, 2, 904.

[11] a) A. V. Prydatko, L. A. Belyaeva, L. Jiang, L. M. Lima, G. F. Schneider, *Nat. Commun.* **2018**, 9, 4185; b) L. Zhang, J. Yu, M. Yang, Q. Xie, H. Peng, Z. Liu, *Nat. Commun.* **2013**, 4, 1443.

[12] A. C. Ferrari, D. M. Basko, *Nat. Nanotechnol.* **2013**, 8, 235.

[13] F. Tuinstra, J. L. Koenig, *J. Chem. Phys.* **1970**, 53, 1126.

[14] a) P. Lespade, A. Marchand, M. Couzi, F. Cruege, *Carbon* **1984**, 22, 375; b) A. Eckmann, A. Felten, I. Verzhbitskiy, R. Davey, C. Casiraghi, *Phys. Rev. B* **2013**, 88, 035426.

[15] a) M. Bruna, A. K. Ott, M. Ijäs, D. Yoon, U. Sassi, A. C. Ferrari, *ACS Nano* **2014**, 8, 7432; b) A. Das, S. Pisana, B. Chakraborty, S. Piscanec, S. Saha, U. Waghmare, K. Novoselov, H. Krishnamurthy, A. Geim, A. Ferrari, *Nat. Nanotechnol.* **2008**, 3, 210; c) Q. H. Wang, C.-J. Shih, G. L. Paulus, M. S. Strano, *J. Am. Chem. Soc.* **2013**, 135, 18866.

[16] M. M. Lucchese, F. Stavale, E. M. Ferreira, C. Vilani, M. Moutinho, R. B. Capaz, C. Achete, A. Jorio, *Carbon* **2010**, 48, 1592.

[17] Z. Zafar, Z. H. Ni, X. Wu, Z. X. Shi, H. Y. Nan, J. Bai, L. T. Sun, *Carbon* **2013**, 61, 57.

[18] A. Eckmann, A. Felten, A. Mishchenko, L. Britnell, R. Krupke, K. S. Novoselov, C. Casiraghi, *Nano Lett.* **2012**, 12, 3925.

[19] a) C. Zhang, L. Fu, N. Liu, M. Liu, Y. Wang, Z. Liu, *Adv. Mater.* **2011**, 23, 1020; b) L. Tang, R. Ji, X. Li, K. S. Teng, S. P. Lau, *J. Mater. Chem. C* **2013**, 1, 4908.

[20] G. Abbas, P. Papakonstantinou, G. R. Iyer, I. W. Kirkman, L. C. Chen, *Phys. Rev. B* **2007**, 75, 195429.

[21] L. Jiang, W. Fu, Y. Y. Birdja, M. T. Koper, G. F. Schneider, *Nat. Commun.* **2018**, 9, 793.

[22] J. W. Suk, A. Kitt, C. W. Magnuson, Y. Hao, S. Ahmed, J. An, A. K. Swan, B. B. Goldberg, R. S. Ruoff, *ACS Nano* **2011**, 5, 6916.

[23] F. Chen, Q. Qing, J. Xia, N. Tao, *Chem. Asian J.* **2010**, 5, 2144.

[24] J.-H. Chen, W. Cullen, C. Jang, M. Fuhrer, E. Williams, *Phys. Rev. Lett.* **2009**, 102, 236805.

[25] A. Ashraf, Y. Wu, M. C. Wang, N. R. Aluru, S. A. Dastgheib, S. Nam, *Langmuir* **2014**, 30, 12827.

[26] B. Blizanac, P. Ross, N. Markovic, *Electrochim. Acta* **2007**, 52, 2264.

[27] A. Sarapuu, K. Helstein, K. Vaik, D. J. Schiffrin, K. Tammeveski, *Electrochim. Acta* **2010**, 55, 6376.

[28] N. Daems, X. Sheng, I. F. Vankelecom, P. P. Pescarmona, *J. Mater. Chem. A* **2014**, 2, 4085.

[29] C. Song, J. Zhang, in *PEM fuel cell electrocatalysts and catalyst layers*, Springer **2008**, p. 89.

[30] a) S. B. Hall, E. A. Khudaish, A. L. Hart, *Electrochim. Acta* **1999**, 44, 4573; b) R. Zhou, Y. Zheng, M. Jaroniec, S.-Z. Qiao, *ACS Catal.* **2016**, 6, 4720; c) S. B. Hall, E. A. Khudaish, A. L. Hart, *Electrochim. Acta* **1998**, 43, 579.